SAND2017-13166C

WAVEFORM OPTIMIZATION FOR RESONANTLY DRIVEN MEMS SWITCHES ELECTROSTATICALLY BIASED NEAR PULL-IN

Aleem M. Siddiqui[1], Christopher D. Nordquist[1], Alejandro Grine[1], Stefan Lepkowsk[1], M. David Henry , Matt Eichenfield[1] and Benjamin A. Griffin[1]
[1]Sandia National Laboratory, Albuquerque, NM, USA

ABSTRACT

Biasing a MEMS switch close to static-pull in reduces the modulation amplitude necessary to achieve resonant pull-in, but results in a highly nonlinear system. In this work, we present a new methodology that captures the essential dynamics and provides a prescription for achieving the optimal drive waveform which reduces the amplitude requirements of the modulation source. These findings are validated both experimentally and through numerical modeling.

INTRODUCTION

Control of closure conditions and nonlinear dynamics of RF-MEMS switches is necessary for many applications including low-power communication, timing, and wake-up signal detection [1-2]. Prior studies have developed necessary requirements for pull-in based on static, transient, and modulated voltage signals [3-4]. Additionally, applying both a static voltage bias and modulated bias to a MEMS switch has been shown to reduce the amplitude requirements needed for the modulated signal [4]. These studies, were developed utilizing a fixed period drive waveform often leveraging resonant actuation. However, for switches positioned exceptionally close to the static pull-in voltage, the dynamics of the switch become extremely nonlinear, and the natural resonant frequency and limit cycle become strongly dependent on the energy stored in the switch. These nonlinear dependences can severely compromise the rate of energy transfer from the modulation waveform to the switch during the course of the switch ring-up. We aim to address these nonlinearities from a theoretical and experimental point of view.

To achieve switch closure with reduced signal levels, we employ resonant actuation with high-Q switches and bias the switch near static pull-in. In the analysis presented in this paper we are interested in how the drive waveform transfers a small amount of energy per cycle to the switch and how the drive waveform can be optimized to minimize the power required of the drive source.For a sufficiently large drive amplitude, the switch will close after many cycles but will essentially sample all possible limit cycle trajectories as a function of energy as it goes from initial ring up to eventual closure.. Since the phase portraits close to pull-in are highly energy dependent, there is an opportunity to optimize the drive waveform to the nonlinear switch response.

We therefore analyze the phase portrait vs energy for the switch and derive approximate expressions for the limit cycle period and quality factor vs energy which captures the prominent increased dwell time as the switch approaches the closure point. We will discuss momentum transfer and amplitude growth which will effectively capture how a drive waveform connects constant energy orbits in phase space. We will also describe how to vary the drive waveform period to match the energy-dependent period of the switch. The theoretical results will be experimentally validated. The hybrid static and dynamic pull-in prescription presented in this work can potentially be exploited for low power signal processing applications dependent on switch closure or "wakeup".

NONLINEAR SWITCH MODEL

A simplified cross-section of the cantilever switch used in this work is shown in Fig 1. The switch is controlled via three electrodes: a bias electrode, a modulation electrode, and a ground electrode. The beam itself is connected to the voltage output or wake-up pad which is grounded through a load resister such that electrostatic forces can be exerted between the control electrodes and the switch body. A DC voltage, V_{DC},is applied to the bias electrode to bring the switch close to pull-in, and a modulated signal, $V_{AC}(t)$, is then applied to the modulation electrode in order to drive the switch to closure.

To investigate the dynamics of the switch, we employ a lumped element model as has been similarly done in prior works [1]. The effects of mass, damping and elastic deformation are captured with linear terms while the electrostatic forces are represented by nonlinear terms. The nonlinear equation for the switch in Fig 1 when driven by separate DC and AC electrodes is given by:

$$m\ddot{x} + b\dot{x} + Kx - \frac{\epsilon_0 A_{DC}}{2(g-x)^2}\times V_{DC}^2 = \frac{\epsilon_0 A_{AC}^2}{2(g-x)^2}\times\frac{V_{AC}^2(t)}{2} \quad (1)$$

where x is the spring displacement, m is the lumped mass, b is the damping coefficient, K is the stiffness, ϵ_0 is the permittivity of free space, $g$is the separation between the spring body and control electrodes, A_{DC} is the bias electrode area, A_{AC} is the modulation electrode area, V_{DC},is the bias voltage, and $V_{AC}(t)$is the applied time dependent modulation voltage. In the above equation, nonlinearities arise from the terms involving V_{DC}^2 and $V_{AC}^2(t)$. The parameters for the switch used in the theoretical and experimental aspects of this work are shown in Fig 1.

In the absence of dissipation and modulation voltage (i.e., $b = 0$ and $V_{AC}(t) = 0$), the resulting homogeneous equation is governed by a potential function, $U(x)$, which can be computed by integrating the elastic and electrostatic force terms on the right hand side of Eq 1.

$$U(x) = \frac{1}{2}Kx^2 - \frac{\epsilon A1}{d_0 - x}\times V_{DC}^2 - U_0 \quad (2)$$

Where U_0 is an arbitrary reference level. $U(x)$ has both a stable position, x_S, and a meta-stable position, x_{MS}, as illustrated in Fig 2. At the stable point the switch position is returned to the stable point for small perturbations. At the meta-stable point, the switch position is driven away from the meta-stable point for small perturbations. Switch closure or pull-in will result if the switch energy, E_{Switch}, exceeds $E_{Close} = U(x_{MS}) - U(x_S)$, the potential energy

difference between the stable and metastable points [1,2]. Furthermore as V_{DC} is increased the distance between the stable point, x_S, and the metastable point, x_{MS}, is reduced and nonlinear behavior resulting from the proximity of the switch to the meta-stable point becomes more prominent. This facts are illustrated in Fig 2. Additionally, the $V_{AC}^2(t)$ term in Eq. 1 indicates that the drive waveform is also subject to a nonlinearity. Thus, to

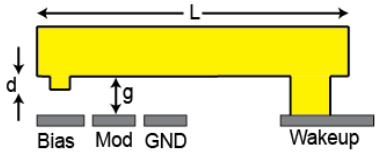

Fig 1: Simplified cross-section of a resonant MEMS cantilever showing the bias, modulation, and ground electrode. The body of the switch is connected to the wakeup pad. For this work the switch parameters are: $f_0 = 25kHz$, $K = 8.14\,N/m$, $Q = 1000$, $d_0 = 1.55\times10^{-6}m$ $A_{RF} = 1\times10^{-9}\,m^2$, and $A_{DC} = 1.5\times10^{-9}\,m^2$.

understand the dynamical closure condition, we are not only interested in the limit-cycle solutions to the homogeneous part of Eq. 1 but also the nonlinearity of the drive term.

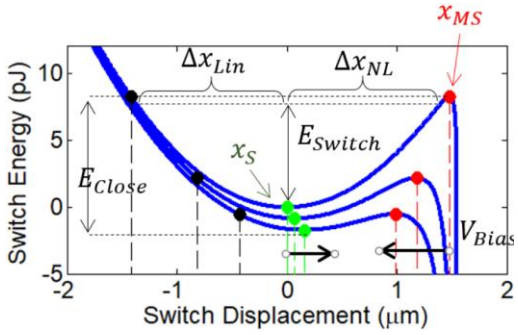

Fig 2: The switch potential well function for various bias voltages near V_{pi}, the pull-in voltage. $x_S$is the stable point and x_{MS} is the metastable point.

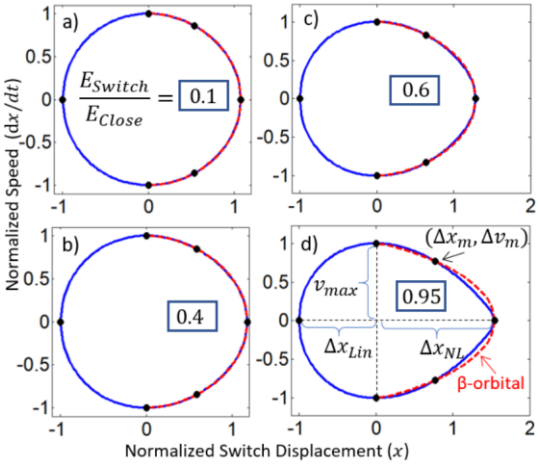

Fig 3: Orbital solutions of constant energy in phase space. The displacement is relative to x_S. And the normalization is done relative to peak speed and maximum displacement when $x < x_S$. The switch energiesfor (a) through (d) are E/E_{close}=.1, .4,.6,.95, respectively. As the energy approaches pull in, the orbital becomes highly asymmetric. The blue curves are numerically integrated orbitals. The red curves are predicted by the analytical formulas discussed in the text.

The phase portrait (x vs dx/dt) as a function of energy captures the essential features of the limit-cycle behavior of the switch as a function of energy. As is typically the case, to construct the phase portrait we neglect the dissipative forceand neglect the driving term. The speed as a function of energy can be solved analytically from conservation of energy. Fig. 3 shows phase portraits corresponding to the various values of switch energy relative to closure energy (E_{Switch}/E_{Close}). As shown in the figure, for low energies, the orbits in phase space are circular indicating that the limit-cycle is essentially harmonic. For large energies, however, the orbit shape becomes highly distorted (Fig 3b) when the switch is in the vicinity of the metastable point. This occurs as the elastic force is partially canceled by the electrostatic force and results in an increased excursion toward the control electrodes as well as an increased dwell time. For $x < x_s$ the phase portrait follows a circular contour even with large switch energy. This suggests that the limit cycle can be viewed as having a harmonic orbit when $x < x_s$ and a nonlinear orbit when $x > x_S$. This is confirmed in Fig 4, which shows that the switch speed is approximately sinusoidal when the switch is in the vicinity of the $x < x_S$ extrema point.

Although the limit cycle behavior is complex, the essential dynamical parameters, namely the period and quality factor, can be extracted from phase space by the following well known relations:[]

$$T(E) = \int \frac{dx}{v(E)}; \quad \frac{Q(E)}{2\pi} = \frac{E}{\int b\frac{dx}{dt}\times\frac{dx}{dt}dt} = \frac{E/b}{A_{LC}(E)} \qquad (3)$$

where E is the switch energy, T is the limit cycle period, $v(E) = dx/dt$ is the energy-dependent switch speed for which an exact formula can be derived from $U(x)$, Q_{NL} is the nonlinear quality factor associated with the limit-cycle when the dissipation term is included, and A_{LC} is the area under the curve of the limit cycle in phase space. The expressions in Eq. 2 depend on integrating $v(E)^{-1}$and $v(E)^2$ for which we do not have closed from integrals. However, for small energies or $x < x_S$, the limit cycle is nearly harmonic (i.e circular orbitals) and is only distorted for large energies and $x > x_S$. In order to have analytical results, we propose to use the following relation for speed to capture this distortion from harmonic motion due to the electrostatic force,

$$v(x) = \begin{cases} v_{max}\left(1-\left(\frac{x}{\Delta x_{LIN}}\right)^2\right)^{\frac{1}{2}}, & x < 0 \\ v_{max}\left(1-\left(\frac{x}{\Delta x_{NL}}\right)^{2+\beta}\right)^{\frac{1}{2}}, & x \geq 0 \end{cases} \qquad (4)$$

where v_{max} is the maximum speed switch speed for a given switch energy, and as noted in Fig 2 and Fig 3d, Δx_{LIN} is the maximum switch displacement for $x < x_S$ when the switch is quasi-linear, while Δx_{NL} is the maximum switch displacement for $x > x_S$. β is a fitting parameter to best match the orbital trajectory in the nonlinear half. The advantage of using Eq.3 is that it leads to expression for $v(E)^{-1}$and $v(E)^2$ which can be integrated analytically.

We outline as follows a prescription to find β for a given switch energy, E_{switch}:

1. We find v_{max} by using the approximation: $E_{switch} =$

$mv_{max}^2/2$

2. We solve for the stable point, x_s, by choosing the appropriate root of the cubic expression: $dU(x_s)/dx = 0$.
3. We solve for $\Delta x_{LIN}, \Delta x_{NL}$, by choosing the appropriate roots for zeros of the cubic function involving the switch potential energy: $U(x) = E_{switch}$.
4. Finally, we solve for the point (x_{mid}, v_{mid}) shown in Fig 3(d) where the switch has half the maximum kinetic energy by choosing the appropriate root of the cubic relation: $U(x_{mid}) = E/4$, nd solving for v_{mid} via conservation of energy. .

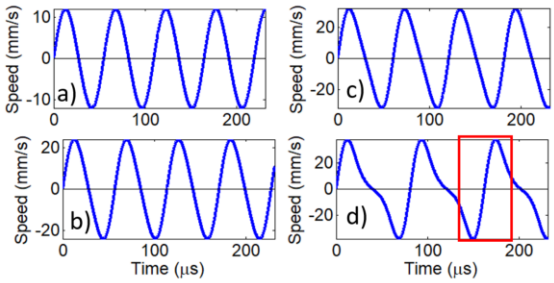

Fig 4: Switch speed vs time corresponding to the limit cycle orbitals in Fig. 2. High energy orbitals experience an increased dwell time close to the metastable point. The red box in (d) indicates harmonic/linear behavior for $x < x_s$

With exact solutions for the above mentioned critical points, we can use Eq (3) to solve for β so that it produces the correct values at (x_{mid}, v_{mid}):

$$\beta(E) = \frac{log\left(1 - \left(\frac{v_{mid}}{v_{max}}\right)^2\right)}{log\left(\left(\frac{x_{mid} - x_0}{\Delta x_{NL} - x_0}\right)\right)} - 2 \quad (4)$$

Thus,by solving a series of cubic expressions and integrating Eq. 3, we arrive at the following expressions for the limit cycle period and quality factor:

$$T(E) = \frac{\pi \Delta x_{Lin}}{v_{max}} + \frac{\Delta x_{NL}}{v_{max}} \frac{2\sqrt{\pi}\Gamma\left(1 + \frac{1}{2+\beta}\right)}{\Gamma\left(\frac{1}{2} + \frac{1}{2+\beta}\right)} \quad (5)$$

$$\frac{Q(E)}{2\pi} = \frac{\frac{1}{2} m {v_{max}}^2 / b}{\Delta x_{NL} \times v_{max} \times \frac{\sqrt{\pi}\Gamma\left(1 + \frac{1}{2+\beta}\right)}{2\Gamma\left(\frac{3}{2} + \frac{1}{2+\beta}\right)} + \frac{\pi}{2} \Delta x_{Lin} \times v_{max}} \quad (6)$$

Fig 3 shows a comparison of the orbitals predicted by the above equations (β-orbitals) to the exact orbitals, and Fig 4 show a comparison of the above expressions to numerically integrated values. The figures confirm that the above expressions capture the essential features of the limit cycle trajectories as a function of switch energy; namely, that the period increases as more energy is stored in the switch and that the quality factor decreases due to the increased dwell time in the vicinity of the applied voltage. In the subsequent sections, we will use these expressions to understand the dynamics of a driven switch.

TRANSIENT DYNAMICS OF DRIVEN SWITCH

The switch is initially at rest and the modulation voltage, $V_{AC}(t)$, will produce a nonlinear driving force through Eq 1 that can increase the switch's motional amplitude and energy. Since the momentum increase and the energy dissipation in Eq 1 are small over the duration of a period compared to the stored energy, the switch motion will be dominated by its limit cycle trajectory on short time scales. On long time scales the switch energy will grow due to momentum transfer or shrink due to dissipation. The goal here is to maximize momentum transfer such that the steady state energy is in excess of the closure energy, E_{Close}, and the switch pulls-in. Put another way, the switch reaches the metastable point shown in Fig 1 and achieve pull-in. Momentum transfer is maximized when the modulation voltage period matches the instantaneous period of the switch, $T(E)$. Thus, the optimal drive waveform for $V_{AC}(t)$ will track the switch period which evolves as the motional amplitude increases. Since power will continue to transfer when the switch is moving in the direction of the metastable point, the optimal drive waveform can be expressed as:

$$V_{AC}(t) = V_0 \times \{v(E(t)) > 0\} \quad (7)$$

In the above equation, $V_{AC}(t)$, is essentially a square wave with voltage applied only when the velocity is positive. The waveform thus tracks the period of the switch as opposed to a square wave with a fixed period.

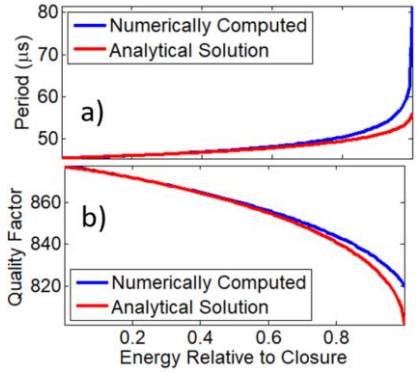

Fig 4: (a) Switch period vs switch energy relative to closure. (b) Switch quality factor vs energy relative to closure. The blue curve is numerically integrated and the red curve is predicated by the equations in the text.

To explore the impact of tracking the switch period we conducted FDTD simulations, the results of which are shown in Fig 5. The switch parameters were chosen to match the switch measured in the experimental section below. Fig 5a shows the transient dynamics of a switch driven to closure with an optimal waveform using feedback (close-looped), and confirms that locally in time the switch motion follows the orbitals predicted in the previous section. Fig 5b shows as a comparison, the switch driven with the optimal waveform and with a fix period waveform. The comparison confirms that more energy is delivered with the optimal waveform, (Eq. 7) resulting in nearly a 5X improvement in steady state switch speed.

When driven with the optimal waveform, Eq. 7, the transient dynamics simplify considerably and are dominated by the momentum transferred per cycle, $p_0(E)$, and the energy dissipated per cycle, $2\pi \times E/Q_{NL}(E)$. If we view the switch as storing an integer amount of momentums, $p_n = N \times p_0$, then the switch energy can be expressed as: $E_n = (N \times p_0)^2$, where N, is the total number of momentums stored and n refers to the cycle iteration.

At a given switch energy, if we assume that in the next cycle a fixed amount of momentum is added and energy is dissipated, a difference equation in terms of energy can be derived:

$$E_{n+1} - E_n = p_0(E_n)\sqrt{\frac{2}{m}\sqrt{E_n}} - \frac{E_n}{Q_{NL}(E_n)/2\pi} \quad (8)$$

In steady state, the energy injected via momentum transfer balances the energy dissipated and we have: $E_{SS} = \frac{1}{2m}\left(\frac{Q_{NL}}{\pi} \times p_0\right)^2$. Thus, in steady state the switch stores Q_{NL}/π momentum quanta, p_0. If p_0 and Q_{NL} were constant Eq 8 would have an analytical solution describing energy exponentially approaching the steady state energy.

The ideas of momentum transfer are explored in Fig 6 which illustrate the nonlinear nature of the momentum transfer. In the figure we are comparing three cases: a switch driven with the optimal wave from, a switch driven with constant momentum transfer of $p_0(E = 0)$, and a switch driven with constant momentum of $p_0(E = E_{SS})$ which matches the steady state momentum transfer of the optimal waveform in steady-state. More specifically, the red curve plots the peak momentum per cycle for a switch driven with the optimal waveform. The black curve plots the peak momentum per cycle of the switch being driven with an impulsive force that

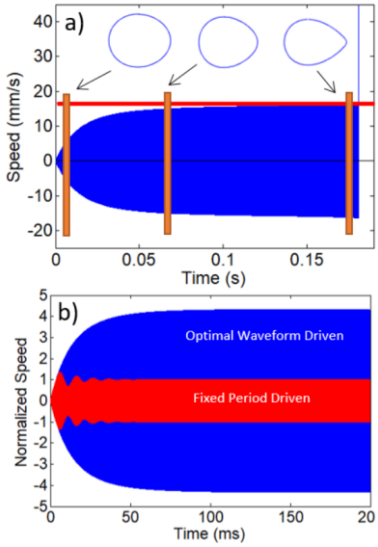

Fig 5: (a) Switch speed as the switch is driven to closure with the optimal waveform. Insets confirm that locally, the switch motion matches predicted orbitals. The red bar is the maximum speed predicted from the closure energy. (b) Switch driven with optimal waveform below closure (blue) vs a fixed period waveform (red). Nearly ×5 improvement in speed is predicted.

delivers the same momentum per cycle as the red curve when initially does when Eswitch=0. The blue curve shows the switch being driven impulsively but the momentum delivered corresponds to the momentum delivered in steady state for the red curve, a switch being driven with the optimal waveform. The solid blue line shows predicted steady state values from Eq 8 using Eq 6., (red line) and assuming only a spring softened Q (blue line).The results of Fig 6 show that steady state. Thus more momentum is transferred per cycle in steady state resulting in more energy stored in the switch. Nearly 30% more energy is delivered to the switch beyond what would have been possible if the initial momentum transfer were maintain. These results show that nonlinear momentum transfer per cycle also plays a role in the switch ring up. Energy can be understood as a balance of momentum transfer and energy dissipation as predicted by Eq 8. However, in steady state momentum transfer increases per-cycle due to the lengthening of the switch period. Eq 6, however, can accurately be used to predict the steady state energy and switch closure.

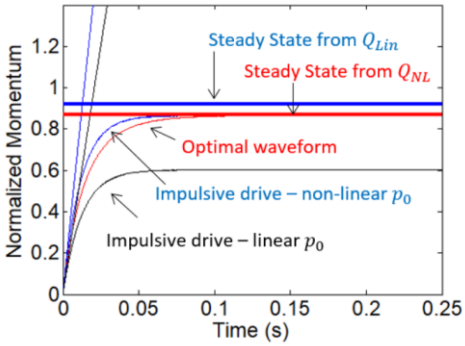

Fig 6: Peak momentum per cycle for switch driven under various conditions describe in the text.

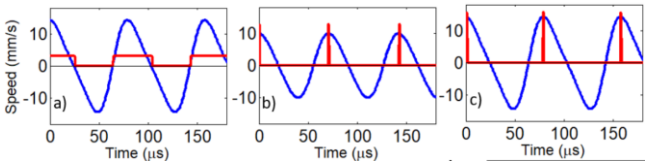

Fig 7: Steady state trajectories for corresponding curves in Fig 6. Switch driven with optimal waveform is shown in (a). Switch driven with impulsive forces are shown in (b) and (c) where the momentum transferred per cycle correspond to a linearized switch and a switch in steady state driven with the optimal waveform, respectively.

SWITCH DESIGN AND FABRICATION

To physically realize the modulated closure/wakeup functionality, we designed and fabricated the cantilever switches shown in Figure 8. The switch body consisted of 5μm thick electroplated gold. To reduce stiction and improve reliability, the electrodes underneath the switch body were fabricated from 100nm thick sputtered Ruthinium Dioxide. We used d=120nm dimple to make contact at the DC bias electrode. The gap between the AC modulation electrode and the body was chosen to be g=360nm. This gap was chosen smaller than traditional RF MEMs switches to reduce the pull-in energy while still allowing enough spring restoring force for the cantilever to re-open after closure.

EXPERIMENTAL VALIDATION

To investigate the switch dynamics experimentally, we developed a test setup capable of driving the switch with either a constant period, or a waveform tracking the changing period. The speed was monitored by a laser Doppler vibrometer (LDV)as shown in Fig 9. As mentioned previously, the optimal power transfer occurs when a drive signal is applied at velocity>0. Therefore, the LDV signal feeds a Schmidt-Trigger comparator circuit and subsequent control electronics to eventually trigger a waveform generator tied to the AC input of the switch. We

describe the drive sequence as follows:, the control electronics initially output a fixed-period square wave for a short duration to initially build up energy in the switch allowing the LDV signal to be detected by the Schmidt-Trigger comparator circuit. After the initial buildup, the comparator output is then used to drive the switch in feedback. The amplitude of the drive waveform is fixed over a drive sequence, and the drive sequence is run long enough in both constant period phase and optimal wave-form mode so that steady state is achieved for both drive types. Additionally, the amplitude of the modulation voltage is stepped up until a switch closure event is recorded. This arrangement allows us to compare the efficacy of the two drive configurations experimentally and match the result to theory.

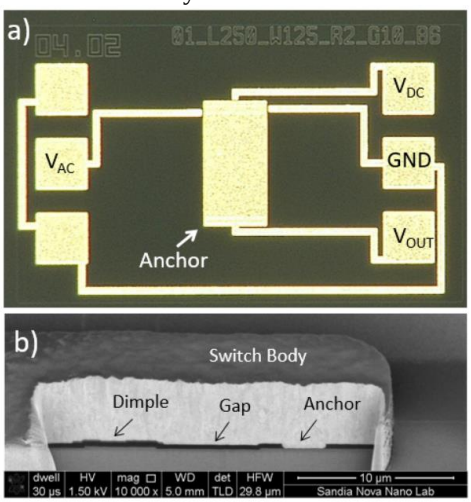

Fig 8: (a) An optical photo-micrograph of a representative MEMS cantilever switch. (b) A cross section of the switch showing the thin sacrificial layer, dimple, and anchor region.

The experimental results are shown in Fig 10, Fig 11, and Fig 12 for a switch with the parameters summarized in Fig 1. The highlighted region Fig 10(a) shows the switch being driven with the initial constant period drive waveform and achieving steady state. After the initial sequence, the switch is shown being driven with the optimal waveform in a closed loop configuration for increasing modulation voltage amplitude. Panel (iv) records the switch closure event and confirms the switch is closed at a reduced signal level and that the closed state is held. Fig 10(b) shows a zoomed in portion of panel (iii) along with the relative phase of the constant drive period and the optimal waveform. This data confirms the ability of our setup to track the switch period We also demonstrate nearly a 5× increase in speed as compared to constant frequency drive confirming the theoretical predictions in the previous sections.

In Fig 11 we match the experimental data to the theoretical framework of the previous section. The Switch period vs switch energy is plotted theoretically as predicted from numerical simulations along with experimental data points, indicating excellent agreement between theory and experimental data. Finally, detailed analysis of the experimental data is shown in Fig 12, where theoretically predicted orbital shapes in phase space match up to experimentally measured data. Additionally the closure event in Fig 10(a) panel (iv) is plotted in phase space, demonstrating the robustness of the analytical model compared to measured data..

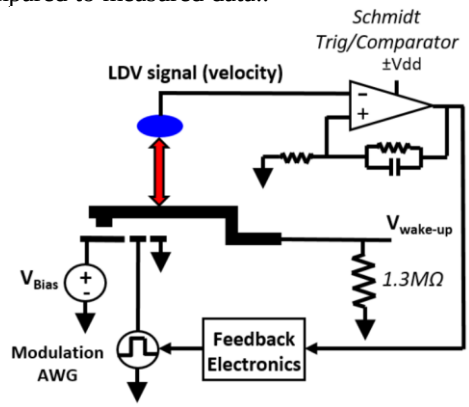

Fig 9: Schematic of experimental setup

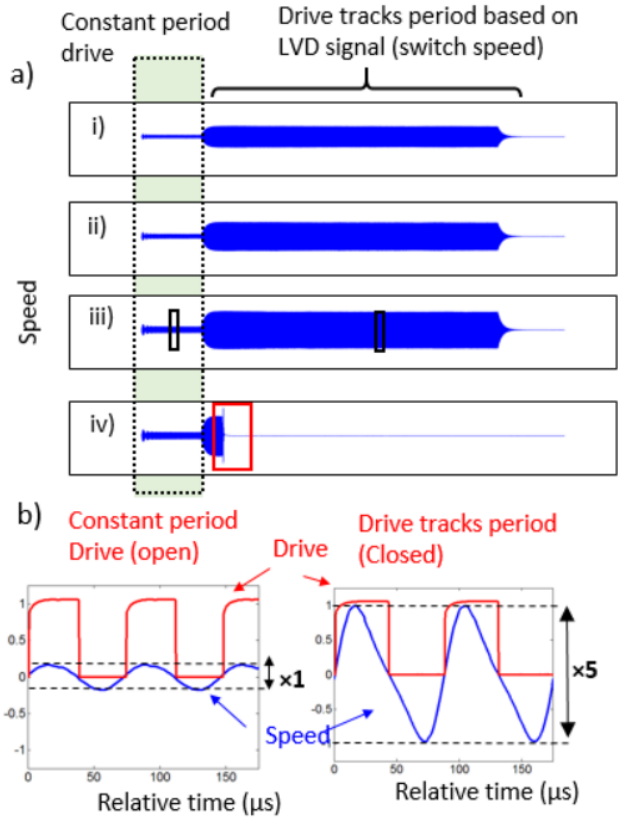

Fig 10: (a) Switch speed measured as the modulation voltage amplitude is increased. Inset iv show the switch closing and staying closed. For each amplitude a constant period drive is used to initially build up energy in the switch. Subsequently a comparator is utilized to drive the switch when the speed has the correct sign, i.e. moving toward the ground electrode. (b) Left corresponds to the left zoomed region in (iii), constant drive, and right corresponds to the right zoomed region in (iii), optimal waveform. The constant-period and optimal drive waveforms are shown in red and the achieved switch speed is shown in blue. Axis ranges are the same in both insets . This illustrates that the optimal waveform is more effective at delivering energy to the switch resulting in 5.5 times more speed.

CONCLUSION

In this work we developed a theoretical framework to analyze the switch dynamics under static, close to pull-in conditions where the switch motion will be strongly influenced by the nonlinear electrostatic forces. We developedclosed-form equations that account for static and dynamic nonlinearities and demonstrated there predictive

capabilities in simulation. The developed theory was additionally validated by an experimental setup and fabricated switches where we found that period-locked drive wave forms weremore effective than fixed-period waveforms at closing the switch. The hybrid static and dynamic pull-in prescription presented in this work can potentially be exploited for low power signal processing applications requiring a wakeup or switch closure.

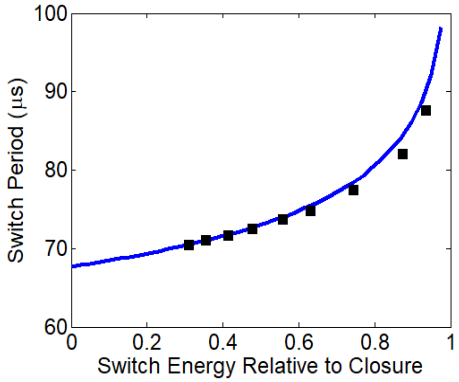

Fig 11. Switch period vs steady state switch energy normalized to closure energy. The blue line corresponds to the switch simulation, and the black squares correspond to experimental data.

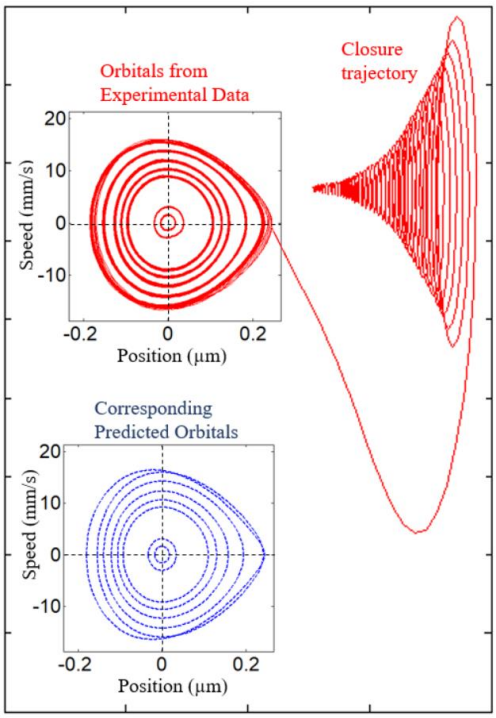

Fig 12. Phase space representation of the steady state orbitals achieved with the optimal drive waveform as the modulated voltage amplitude is increased until closure. The red curve is experimental while the blue curve corresponds to predicted orbitals. The extended trace at right corresponds to the switch closure event.

ACKNOWLEDGEMENTS

Sandia National Laboratories is a multi program laboratory managed and operated by Sandia Corporation, a wholly owned subsidiary of Lockheed Martin Corporation, for the U.S. Department of Energy's National Nuclear Security Ad-ministration under contract DE-AC04-94AL85000.

Sandia National Laboratories is a multi-mission laboratory managed and operated by NTESS of Sandia, LLC., a wholly owned subsidiary of Honeywell International, Inc., for the U.S. Department of Energy's National Nuclear Security Administration under contract DE-NA0003525. This work was supported by the DARPA N/ZERO Program, program manager Linton Salmon (Troy Olsson) and by the Laboratory Directed Research and Development Program. The views, opinions, and/or findings expressed are those of the author(s) and should not be interpreted as representing the official views r policies of the Department of Defense or the U.S. Government. The authors acknowledge fabrication support by the Sandia MESA-Fab operations team and test and measurement support by M. Ballance, S. Habermehl, B. Hunt, R. Reger, M. Satches, and A. Schiess.

REFERENCES

[1] Nielson, G. N., and G. Barbastathis. "Dynamic Pull-in of Parallel-Plate and Torsional Electrostatic MEMS Actuators." *Journal of Microelectromechanical Systems* 15, no. 4 , pp. 811–21, 2006.

.[2] Fargas-Marques, A., J. Casals-Terre, and A. M. Shkel. "Resonant Pull-In Condition in Parallel-Plate Electrostatic Actuators." Journal of Microelectromechanical Systems 16, no. 5, pp: 1044–53, 2007.

[3] Juillard, Jérôme. "Analysis of Resonant Pull-in of Micro-Electromechanical Oscillators." Journal of Sound and Vibration 350 (August 18, 2015): 123–39.

[4] Alsaleem, F. M., M. I. Younis, and L. Ruzziconi. "An Experimental and Theoretical Investigation of Dynamic Pull-In in MEMS Resonators Actuated Electrostatically." Journal of Microelectromechanical Systems 19, no. 4 (August 2010): 794–806..

[5] Zhang, W. M., and G. Meng. "Nonlinear Dynamic Analysis of Electrostatically Actuated Resonant MEMS Sensors Under Parametric Excitation." IEEE Sensors Journal 7, no. 3 (March 2007): 370–80. [3]

[6] Brenes, A., J. Juillard, L. Bourgois, and F. Vinci Dos Santos. "Influence of the Driving Waveform on the Open-Loop Frequency Response of MEMS Resonators With Nonlinear Actuation Schemes." Journal of Microelectromechanical Systems 25, no. 4 (August 2016): 812–20.

[7] Liu, J., D. T. Martin, T. Nishida, L. N. Cattafesta, M. Sheplak, and B. P. Mann. "Harmonic Balance Nonlinear Identification of a Capacitive Dual-Backplate MEMS Microphone." Journal of Microelectromechanical Systems 17, no. 3 (June 2008): 698–708.

[9] LWu, T., G. Chen, Z. Qian, W. Zhu, M. Rinaldi, and N. McGruer. "A Microelectromechanical AlN Resoswitch for RF Receiver Application." In 2017 19th International Conference on Solid-State Sensors, Actuators and Microsystems (TRANSDUCERS), 2123–26, 2017. 494.

[10] LWu, T., G. Chen, Z. Qian, W. Zhu, M. Rinaldi, and N. McGruer. "A Microelectromechanical AlN Resoswitch for RF Receiver Application." In 2017 19th International Conference on Solid-State Sensors, Actuators and Microsystems (TRANSDUCERS), 2123–26, 2017. 494.

[11].R.Liu, J. Naghsh Nilchi, Y. Lin, T. L. Naing, and C. T. C. Nguyen. "Zero Quiescent Power VLF Mechanical Communication Receiver." In 2015 Transducers - 2015 18th International Conference on Solid-State Sensors, Actuators and Microsystems (TRANSDUCERS), 129–32, 2015.

CONTACT

*A.M.Siddiqui, asiddiq@sandia.gov